Materials Advances

ROYAL SOCIETY OF CHEMISTRY

PAPER

View Article Online
View Journal | View Issue

Cite this: *Mater. Adv.*, 2023, 4, 2595

Ni(II) and Zn(II)-metallogel-based anti-bacterial scaffolds for fabricating light-responsive junction-type semiconducting diodes with non-ohmic conduction mechanism†

Gerald Lepcha,[a] Baishakhi Pal,[b] Santanu Majumdar,[a] Kazi Tawsif Ahmed,[c] Indrajit Pal,[a] Swadesh Ranjan Biswas,[c] Partha Pratim Ray *[b] and Biswajit Dey *[a]

Metal incorporation into the gelator offers an effective strategy to fabricate soft scaffolds with advanced functionality. Herein, we report self-assembly directed two supramolecular metallogels of sebacic acid with Ni(II) and Zn(II) metal salts. *N*,*N*′-dimethyl formamide (DMF) solvent was immobilized within metallogel-scaffolds. Distinct features with diverse morphological patterns as an outcome of versatile supramolecular interactions operating within gel-scaffolds, *viz.*, Ni(II)–sebacic acid (**Ni–SB**) and Zn(II)–sebacic acid (**Zn–SB**) were achieved. Both of these metallogels display a visco-elastic nature that was experimentally visualized by means of rheological parameters. To visualize reversible, isothermal, time-dependent sol–gel transitions for both metallogels, thixotropy measurements were performed and the experimental outcome confirmed the thixotropic nature of these reported metallogels. FESEM micro-structural imaging of both metallogels was conducted and revealed dissimilar morphological patterns. Possible non-covalent interactions involved within the metallogel scaffolds were analyzed *via* FT-IR studies. Both of these metallogels were comparatively studied for their antibacterial activity against human pathogens of Gram-negative and Gram-positive bacteria. Antibacterial activity of both metallogel-scaffolds were tested against *Klebsiella pneumoniae* (MTCC 109), *Vibrio parahaemolyticus, Bacillus cereus* (MTCC 1272), and *Staphylococcus aureus* (MTCC 96). Relative analysis of the antibacterial aspect of both metallogels towards the aforesaid pathogens reveals that **Zn–SB** may be a better candidate. MIC for **Ni–SB** was found to be ~300 μg mL^{-1} for Gram-positive bacteria, which is approximately 4-fold higher than that of **Zn–SB**. Apart from the biological significance, these metallogels were utilized for junction-type Schottky-diode device fabrication through sandwich configuration along with the ITO/compound/Al structure. The device fabricated by means of both metallogels exhibits non-ohmic type electrical conduction. The device fabricated by means of **Ni–SB** exhibits a larger current density under dark conditions than **Zn–SB**. However, in the presence of light, the device based on **Zn–SB** shows a higher on/off ratio with respect to **Ni–SB**.

Received 29th January 2023,
Accepted 18th April 2023

DOI: 10.1039/d3ma00054k

rsc.li/materials-advances

1. Introduction

Many examples of supramolecular phenomena exist in Nature. Studies on these non-covalent interactions unveil its fundamental significance and crucial role over innumerable natural instances.[1] Inspired from these essential and abundant valuable efforts of supramolecular chemistry, modern research chemists are devoted to expanding this exciting domain in the laboratory. "Metallo supramolecular self-assembly"[2] is a significant dimension of scientific area that has emerged owing to its active control over host–guest moieties,[3] size-selective entrapment,[4] stereo-selective chemical reactions,[5] supramolecular polymers,[6] *etc.* Self-assembly-directed supramolecular gelation with its innovative insight delivers a valuable platform for advanced future technologies.[7–9] Assimilation of metal components into gel scaffolds offers an effective approach to advance soft materials with beneficial functionalities, such as electrical and thermal conductivity,[10–14] optical properties,[15,16] stimuli-responsive magnetism,[17–20] self-healing behavior,[16,17,21–23] catalytic action,[24–27] antibacterial property,[28–32] sensing,[33–40] and redox properties.[35,41,42] Besides these added benefits, metal incorporation establishes added interactions within the building blocks that help to trigger gelation,[43–47] modifying morphological patterns,[48,49] and consequently enhance[50,51] or weaken[52] the mechanical features of

[a] *Department of Chemistry, Visva-Bharati University, Santiniketan 731235, India. E-mail: bdeychem@gmail.com; Tel: +91 9433868381*
[b] *Department of Physics, Jadavpur University, Kolkata 700032, India. E-mail: parthap.ray@jadavpuruniversity.in*
[c] *Department of Botany, Visva-Bharati University, Santiniketan-731235, India*

† Electronic supplementary information (ESI) available. See DOI: https://doi.org/10.1039/d3ma00054k

gel materials. The integration of specific properties of metal ions with gelators appears as an effective strategy to tune the aforesaid properties to have a functional metallogel. The elegant choice of metal ions and the design of versatile gelator molecules, along with choosing the appropriate solvent, are incredibly crucial facets in terms of building gel architectures. The aspect of metal–ligand interactions is one of the vital driving forces for gelation.[53–56] Macroscopic *vis-a-vis* microscopic characteristics of gel-scaffolds are reliant on the nature of its constituting chemical components.

The metallogel consists of uniquely interlinked three-dimensional networks with solvent encapsulation through several non-covalent interactions operating among the gelling components of metal salts and organic gelators. The design and fabrication of a metallogel utilizing a low molecular weight gelator (LMWG) are of profound interest owing to multiple aspects, such as versatility, easy availability, good solubility and inducing smooth gelation even at very low concentration, cost effectiveness, among others.[57–59] Literature reports on LMWGs highlight molecules with specific organo-functional groups, such as carboxylic acids,[16,17,60–65] amines,[17,66–68] amino acids,[59] N-donating heterocyclic components like triazole,[69] tetrazole,[70,71] and others, as tremendously fruitful in terms of their gelling characteristic features. Interactions operating among the LMWG molecules provide 1D fibrillar networks that entangle among themselves to form a 3D network called self-assembled fibrillar networks (SAFiNs). Thus, the solvent immobilization occurs directly to produce a gel.[72] Various morphological patterns arising in gel-materials due to the variety of aggregations guided through interactions involving electrostatic, π–π stacking, hydrophobic and hydrophilic interactions, van der Waals interactions, and hydrogen bonding interactions are well documented.[2,16] Moreover, the principal requirement for the fabrication of gel-like scaffolds is a gelator molecule with active sites, which can participate in supramolecular interactions. Pioneering efforts utilizing the metallogel serving as a template for designing advanced materials with superior functionality as quantum dots, nanorods, 3D networks, and chiral materials are well documented.[73] There is rapid progress in the focused development of metallogels on the basis of its utility in biological applications, such as wound healing,[31] drug delivery,[20,30,74] anti-cancer, and anti-tumor,[28,75] anti-inflammation,[76] and tissue engineering.[18] Tao *et al.* reported an *in situ* self-assembly driven supramolecular metallogel of Zn(II) and peptide that is useful for drug delivery, offering the treatment of prostate cancer.[77] Some of the well-known significant functionalities of sebacic acid towards the synthesis of bio-elastomers and biodegradable hydrogels for tissue engineering,[78,79] a major inorganic component like the hydroxyapatite found in bone minerals,[80] graphite composite phase-change material for thermal energy storage,[81] bio-based copolyesters utilized for food packaging,[82] sensitive adhesives,[83] have been documented. These literature observations motivated us to explore the possibility of offering the Ni(II) and Zn(II)-based bio-relevant metallogel-systems of sebacic acid for use as the low molecular weight organic gelator. Apart from the biological significances of sebacic acid, LWMGs-based gels also provide flexible scaffolds required for smooth electron transport. Hence, these supramolecular gel systems can be utilized for fabricating semiconducting diodes. This article highlights the design, fabrication, antibacterial activity and electrical characterization in terms of the junction-type Schottky diode nature of two supramolecular metallogel-based systems consisting of sebacic acid with Ni(II) and Zn(II) metal salts. DMF solvent was used for the fabrication of both metallogels. Experimental findings in terms of the minimum critical gelation schemes between the two metallogels show that Ni(II) acetate tetrahydrate offers more effective and efficient gelation than Zn(II) acetate dihydrate. Rheological analyses were carried out for both metallogels. The outcome of these rheological findings verifies that the synthesized materials are thixotropic in nature, which was measured for both metallogels. These findings support the reversible, isothermal, time dependent sol–gel transitional behavior for both of these metallogels. Micro-structural patterns of both metallogels were visualized through FESEM analysis. Both metallogels display distinct morphological scenarios. Involvement of possible noncovalent supramolecular interactions within the xerogel scaffolds were carefully analyzed by means of shifting of infrared spectral analysis with respect to the LMWG, *i.e.*, sebacic acid. Both supramolecular metallogels were comparatively studied for antibacterial activity against human pathogens, including Gram-negative and Gram-positive bacteria. The antibacterial activity of both metallogel scaffolds were studied against *Klebsiella pneumoniae* (MTCC 109), *Vibrio parahaemolyticus, Bacillus cereus* (MTCC 1272), and *Staphylococcus aureus* (MTCC 96). The **Zn–SB** metallogel was found to be more effective in terms of antibacterial activity than **Ni–SB** against the abovementioned pathogens. The MIC for **Ni–SB** was found to be $\sim$300 μg mL^{-1} for Gram-positive bacteria, which is approximately 4-fold higher than that of **Zn–SB**.

Apart from their biological significance, these metallogels were utilized for junction-type Schottky diode device-fabrication through sandwich configuration along with an ITO/metallogel/Al structure. The device fabricated by means of both metallogels exhibits non-ohmic type electrical conduction. The electrical characterization was carried out at room temperature. The nature of the *J–V* characteristics is similar for both gel samples (*i.e.*, **Ni–SB** and **Zn–SB**), with the directed devices exhibiting a considerable amount of non-linearity in the scanned voltage range except for the current density, implying a non-ohmic conduction mechanism. This characteristic feature is similar to that of the Schottky barrier diode's rectification. The device performances of the **Ni–SB** and **Zn–SB**-based systems in terms of the electrical parameters vary under dark and light stimulation. The device fabricated by means of the **Ni–SB**-based system exhibits a larger current density than that of the **Zn–SB** system under a dark environment, whereas the device based on **Zn–SB** shows a higher on/off ratio with respect to **Ni–SB** in the presence of light.

2. Experimental section

2.1. Materials

Nickel(II) acetate tetrahydrate, nickel(II) chloride hexahydrate, nickel(II) nitrate hexahydrate, nickel(II) sulphate hexahydrate, zinc(II) acetate dihydrate, zinc(II) chloride, zinc(II) nitrate

hexahydrate, zinc(II) sulphate heptahydrate, sebacic acid, DMF, benzene, acetonitrile, tetrahydrofuran, chloroform, ethyl acetate, methanol, ethanol, dichloromethane, acetic acid, acetone, and petroleum ether were procured for utilization from Sigma Aldrich Company. DMF was distilled before its use in synthetic purpose.

2.2. Characterizations

Rheological analyses of these two metallogels were performed with an AntonPaar rheometer (MCR 102). Morphological patterns were visualized by means of field emission scanning electron microscopy (FESEM) *via* a (ZEISS (Gemini 2) Gemini-SEM 450 field emission scanning electron microscope. Microstructural analyses and EDX elemental mapping were investigated through an EDAX (AMETEK MODEL: ELEMENT) instrument. IR spectral analyses of Xerogels and gel forming constituents were investigated by employing a PerkinElmer made spectrometer. The current density–voltage (*J–V*) characteristic was calculated with a Keithley 2635B source meter by two-probe technique to obtain the electrical parameters of the device.

2.3. Synthetic protocol for sebacic acid-based metallogels of Ni(II) (Ni–SB) and Zn(II) (Zn–SB)

The directed self-assembly of these two metallogels was conducted at room temperature employing DMF solvent. The minimum critical gelation was precisely carried out for both metallogels to determine the minimum gel forming concentration for both cases. In order to synthesize the **Ni–SB** metallogel, $Ni(CH_3COO)_2{\cdot}4H_2O$ (49.8 mg mL^{-1}) 0.2 mmol and sebacic acid (40.4 mg mL^{-1}) 0.2 mmol were each taken in 1 mL DMF in two separate beakers. Clear homogeneous solutions were achieved by means of mechanical stirring. These two solutions were mixed in a glass vial, and an instant green-coloured metallogel formation was observed. Preliminary observation with an ''inversion vial test'' was conducted to assure its stability against the gravitational force. Following the similar synthetic protocol, a white-coloured Zn(II)–Sebacic acid metallogel was synthesised. The **Zn–SB** metallogel was fabricated with $Zn(OAc)_2{\cdot}2H_2O$ (328.5 mg mL^{-1}) 1.5 mmol and sebacic acid (303 mg mL^{-1}) 1.5 mmol. The synthetic process of the **Ni–SB** and **Zn–SB** metallogels are shown in Scheme 1. The metallogelation process for both metallogels was examined with a variety of other salts, such as $NiCl_2{\cdot}6H_2O$, $Ni(NO_3)_2{\cdot}6H_2O$, $NiSO_4{\cdot}6H_2O$, $ZnCl_2$, $Zn(NO_3)_2{\cdot}6H_2O$ and $ZnSO_4{\cdot}7H_2O$, along with sebacic acid maintaining the optimum concentration as mentioned in the synthetic scheme. None of these salts were able to produce the targeted metallogel. This experiment suggests that Ni(II) and Zn(II) metal ions with acetate as counter anions are highly efficient and effective towards the metallogelation process (For details, please see ESI† Fig. S1 and S2).

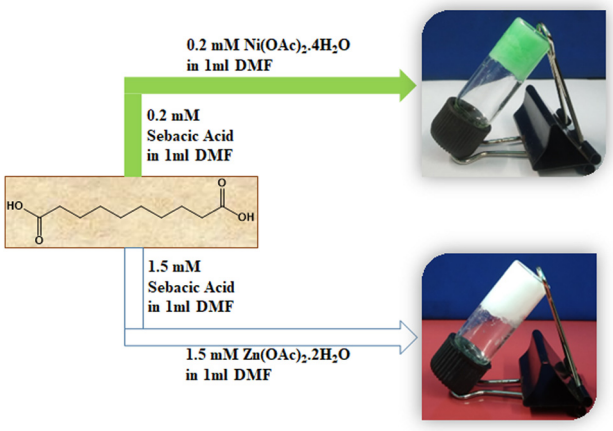

Scheme 1 Pictorial representation of the synthetic process for **Ni–SB** (green-coloured) and **Zn–SB** (white-coloured) metallogels.

2.4. Minimum critical gelation concentration (MCG) of the synthesized Ni–SB and Zn–SB metallogels

The minimum critical gel forming concentrations (MCG) of the **Ni–SB** and **Zn–SB** metallogels were carefully visualized. For all sebacic acid-directed metallogels, the concentrations of the gel-forming chemical-components, *i.e.*, $Ni(CH_3COO)_2{\cdot}4H_2O$, $Zn(CH_3COO)_2{\cdot}2H_2O$ and sebacic acid, were retained as 1 : 1, w/w. The premium class of supramolecular metallogel **Ni–SB** was observed when the concentrations of Ni(II)-salt and sebacic acid were taken as 49.8 and 40.4 mg mL^{-1}, respectively. Whereas for the supramolecular **Zn–SB** metallogel, the finest quality of gel was visualized when the concentrations of the Zn(II)-salt and sebacic acid were taken as 328.5 and 303 mg mL^{-1}, respectively. Comparative analyses of MCG of these two metallogels clearly illustrate that **Ni–SB** formation occurs at a very low concentration. This experimental fact clearly suggests that the Ni(II)-salt is very efficient towards metallogelation with sebacic acid among these two metal salts (For details, please see ESI,† Tables S1, S2 and Fig. S3, S4). Thus, metallogels with lower values of MCG are very efficient and effective towards the metallogelation process.

2.5. Determination of the optimum solvent for achieving stable metallogels of Ni–SB and Zn–SB

The gel forming ability of different solvents ranging from non-polar to polar classes were verified experimentally to acquire the stable metallogels of **Ni–SB** and **Zn–SB**. The conclusion of this experimental result clearly validates that *N*,*N*′-dimethyl formamide (DMF) is the best suitable solvent to achieve the stable **Ni–SB**, and **Zn–SB** metallogels under ambient experimental conditions (For details, please see ESI,† Fig. S5 and S6).

2.6. Inhibiting activity of Ni–SB and Zn–SB towards deadly bacterial pathogens

Both of these supramolecular metallogels, Ni(II)–Sebacic acid and Zn(II)–Sebacic acid, were tested for their antibacterial potentiality against Gram-negative bacteria, *viz.*, *Klebsiella pneumoniae* (MTCC 109), *Vibrio parahaemolyticus* and Gram-positive bacteria, *viz.*, *Bacillus cereus* (MTCC 1272), and *Staphylococcus aureus* (MTCC 96), subsequently employing the technique as reported by Biswas *et al.*[84]

3. Results and discussion

3.1. Rheological experimental analysis of Ni–SB and Zn–SB Metallogels

AntonPaar Compact Modular Rheometer (MCR 102) Parallel Plate 25 (PP25) was utilised to verify the mechanoelastic characteristic features of the **Ni–SB** and **Zn–SB** metallogels. The entire rheological parameters were extracted at a constant temperature of 25 °C. A precise Peltier device assured fixed temperature. For both gel samples, amplitude sweep experiments were conducted at constant angular frequency (ω), *i.e.*, 10 rad/sec, maintaining a range limit of 0.01% to 100% shear strain for both **Ni–SB** and **Zn–SB**. The crossover point of the storage modulus (G') and loss modulus (G'') occurs at 3.83% and 5.41% shear strain for the **Ni–SB** and **Zn–SB** metallogels, respectively (Fig. 1a and b).

The viscoelastic nature of both metallogels was examined by means of frequency sweep experiments. The dependence of storage modulus (G') and loss modulus (G'') parameters with angular frequency for the **Ni–SB** and **Zn–SB** metallogels were analysed (Fig. 1c and d). These experiments were conducted within an angular frequency limit of 100 rad s^{-1} to 0.1 rad s^{-1}. For both metallogels, no entanglement effect was observed in this range. The storage and loss moduli parameters seem to be approximately parallel with each other for both metallogels. This demonstrates that our synthesised materials **Ni–SB** and **Zn–SB** possess characteristic properties of gel-scaffolds.

Besides the viscoelastic nature, these metallogels are thixotropic in nature. Thixotropy refers to time-dependent viscosity. For gel-scaffolds, it implies a reversible isothermal sol–gel transition in the presence of an external stimulus. Upon external mechanical force or agitation, the gel experiences a conversion to the sol state, and regenerates back to its gel upon the withdrawal of external stimuli. Non-Newtonian pseudo fluids are a class of materials that exhibit thixotropic behaviour.

Time sweep experiments were performed to visualize the thixotropic nature of the gel samples. Sequential application of

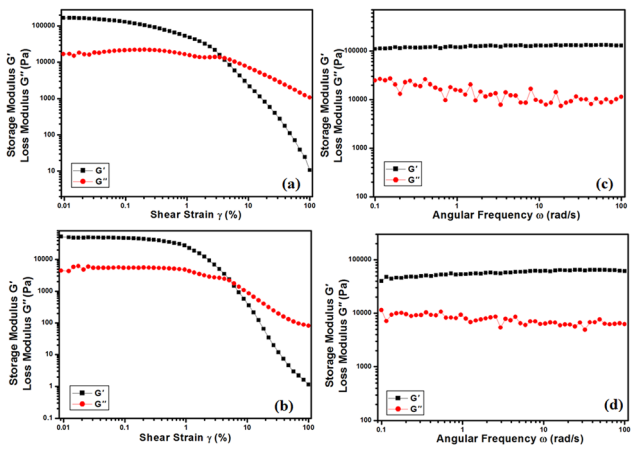

Fig. 1 Rheology data of metallogels showing (a) strain sweep of **Ni–SB**, (b) strain sweep of **Zn–SB**, (c) frequency sweep of **Ni–SB** and (d) frequency sweep of **Zn–SB**.

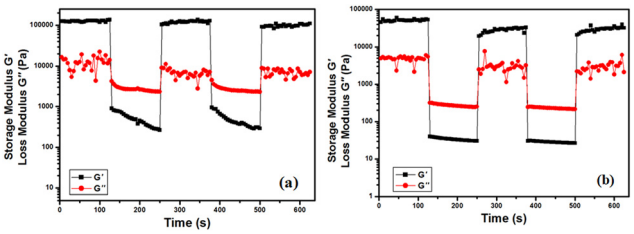

Fig. 2 Time sweep experiments for (a) **Ni–SB** and (b) **Zn–SB**.

low and high shear strain separated by enough time to fulfill reversible sol–gel transitions were achieved for both metallogels (Fig. 2a and b).

Time sweep experiments were initiated at 0.01% shear strain. The metallogels were completely altered to the quasi-liquid state (sol) in the presence of high strain. This is evident from the time sweep plots of both metallogels, *i.e.*, ($G' < G''$). Furthermore, both metallogels were regenerated and examined *via* time sweep experiment under the presence of 0.01% strain, and the modulus parameters support the re-establishment of the gel ($G' > G''$). Again, the metallogels were ruptured and recovered in another stage. These experiments were performed at 10 rad s^{-1} angular frequency (ω).

3.2. FESEM microstructural analysis and experimental outcomes

Microstructural analyses of xerogel samples of these metallogels were collected through FESEM in order to visualize the morphological patterns arising from the supramolecular interactions among the gel-forming constituents. Careful visualization through FESEM of the Ni(II)–Sebacic acid (**Ni–SB**) metallogel reveals the characteristic self-assembled three-dimensional building blocks with inter-connected arrangements of dissimilar-type bolder-shaped structure observed in the μm range. This observed morphological pattern in the **Ni–SB** metallogel is critically responsible for the immobilization of the polar solvent DMF within its framework. The presence of organic constituents, such as carbon and oxygen of sebacic acid, Ni, carbon, and oxygen derived from $Ni(CH_3COO)_2{\cdot}4H_2O$, as well as the role of nitrogen arising from the source of DMF, were examined experimentally through EDX elemental analysis (Fig. 3).

For the zinc–sebacic acid metallogel (**Zn–SB**), the fascinating interconnected three-dimensional network, built by the hierarchically stacked flakes-like morphological pattern, was visualized. The possible non-covalent supramolecular interactions operating within the gel-forming chemical constituents are critically responsible for such observed hierarchical pattern with self-assembled nano-dimensional flakes (Fig. 4). EDX elemental analysis results confirm the existence of organic constituents as carbon and oxygen of sebacic acid, and zinc, carbon, and oxygen derived from $Zn(CH_3COO)_2{\cdot}2H_2O$, alongside nitrogen from the source of DMF in gel scaffolds (Fig. 4).

3.3. Infrared spectroscopic study

Infrared spectroscopic analysis of the xerogel samples obtained from **Ni–SB** and **Zn–SB** was carefully performed. The underlying

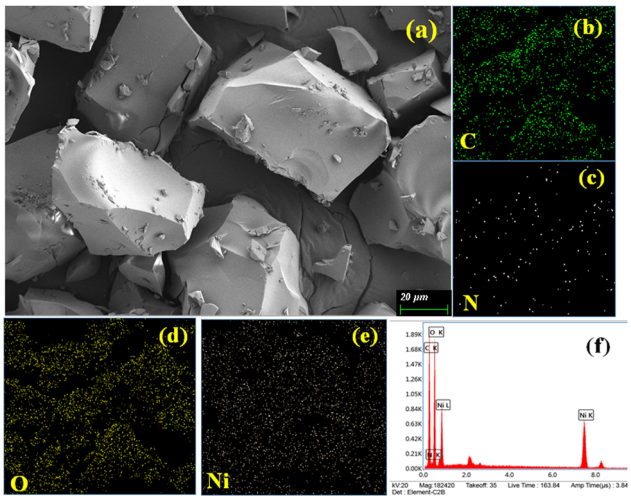

Fig. 3 (a) FESEM microstructural patterns of the **Ni–SB** metallogel; (b–e) elemental mapping of **Ni–SB** highlighting the presence of C, N, O, and Ni elements as the constituents of the **Ni–SB** metallogel; (f) EDX spectrum for the **Ni–SB** metallogel.

significance of different metallogel-forming constituents, involved as a basis of metal-salts (*i.e.*, $Ni(OAc)_2{\cdot}4H_2O$, and $Zn(OAc)_2{\cdot}2H_2O$), metal-incorporating organic gelator like sebacic acid, and the immobilized solvent (*N*,*N*-dimethyl formamide) for the synthesis of **Ni–SB**, and **Zn–SB** metallogels was examined critically by FT-IR study, which clearly showed a considerable shift in the FT-IR peak-patterns in the xerogel samples obtained from these metallogels. Some of the major IR spectral peaks (Fig. 5a) obtained from the xerogel samples from the **Ni–SB** metallogel are detected at 2924 cm^{-1}, 2852 cm^{-1}, 1664 cm^{-1}, 1570 cm^{-1}, 1413 cm^{-1}, 1310 cm^{-1}, 1266 cm^{-1}, 1104 cm^{-1}, 925 cm^{-1}, 876 cm^{-1}, 723 cm^{-1}, 683 cm^{-1}, and 620 cm^{-1}. Similarly, for the **Zn–SB** metallogel, the major peaks

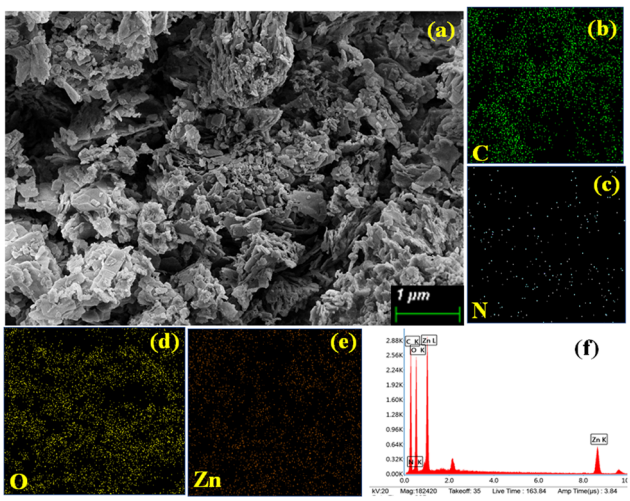

Fig. 4 (a) FESEM microstructural patterns of the **Zn–SB** metallogel; (b–e) elemental mapping of **Zn–SB** highlighting the presence of C, N, O, and Zn elements as the constituents of the **Zn–SB** metallogel; (f) EDX spectrum of the **Zn–SB** metallogel.

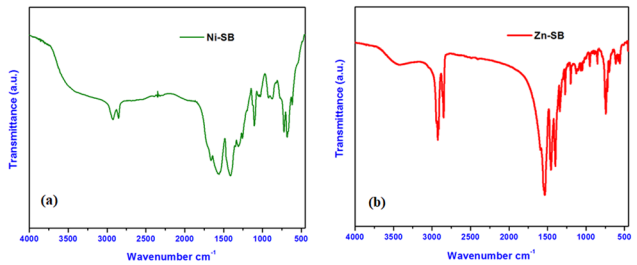

Fig. 5 Infrared spectral data of the xerogel samples of (a) **Ni–SB** and (b) **Zn–SB** metallogels.

are obtained at 2927 cm^{-1}, 2856 cm^{-1}, 1538 cm^{-1}, 1457 cm^{-1}, 1403 cm^{-1}, 1340 cm^{-1}, 1273 cm^{-1}, 1197 cm^{-1}, 951 cm^{-1}, 852 cm^{-1}, 744 cm^{-1}, 700 cm^{-1}, and 618 cm^{-1} (Fig. 5b). For sebacic acid, the peaks were obtained at 2936 cm^{-1}, 2856 cm^{-1}, 1697 cm^{-1}, 1455 cm^{-1}, 1431 cm^{-1}, 1352 cm^{-1}, 1302 cm^{-1}, 1239 cm^{-1}, 1187 cm^{-1}, 1049 cm^{-1}, 931 cm^{-1}, 755 cm^{-1}, 724 cm^{-1}, 678 cm^{-1}, and 551 cm^{-1} (Please see ESI† for the IR spectra of pure sebacic acid given as Fig. S7). Most of the recorded values obtained from the xerogel samples of metallogels **Ni–SB** and **Zn–SB** are lower than that of the experimental values, as obtained from the constituents involving sebacic acid and previously reported results of the pure forms of the respective metal salts, like $Ni(OAc)_2{\cdot}4H_2O$ and $Zn(OAc)_2{\cdot}2H_2O$.[16,60] All of the observations might be critically accountable for the non-covalent type supramolecular interactions involved within the construction of different metallogel networks.

3.4. Study of the antibacterial activity of Ni–SB, and Zn–SB

Antibacterial activities of these two metallogels, *viz.*, **Ni–SB** and **Zn–SB**, against the said pathogens were critically analysed. These two metallogels at a concentration of 100 mg mL^{-1} were suspended in sterile Milli-Q water to achieve homogeneous solutions. A total volume of 5 μL of the gel suspensions was initially spotted into the lawn of the aforesaid bacteria in TGE (tryptone, glucose, and yeast extract, all at 1%; pH 6.5) agar plate.[85–87] These plates were incubated overnight, maintaining the temperature at 37 °C to elicit the zone of growth inhibition. Ampicillin (50 μg mL^{-1}) was also verified as a positive control.

The minimum inhibitory concentration (MIC) for both metallogels **Ni–SB** and **Zn–SB** was carefully examined. Various concentrations of **Ni–SB** and **Zn–SB** metallogel suspensions (50, 75, 100, 150, 200, 300, 500, 1000 μg mL^{-1}) were taken in cultures at 0 h. Culture growth was then observed spectrophotometrically (OD-600). In order to visualize the mode of action of the synthesized metallogels (*i.e.*, **Ni–SB** and **Zn–SB**), bacterial growth was allowed in TGE medium, and the individual metallogel suspensions were added systematically at the obtained MIC. The culture growth was checked spectrophotometrically (OD-600), and the cultures were serially diluted up to 10^{-4} times. Furthermore, they were allowed to spread on the TGE-agar plate. These plates were then incubated for the entire night at 37 °C to allow for growth.

After careful analysis of the antibacterial prospects of the metallogels (*i.e.*, **Ni–SB** and **Zn–SB**), both metallogels were found to be effective against Gram-positive bacteria *B. cereus*,

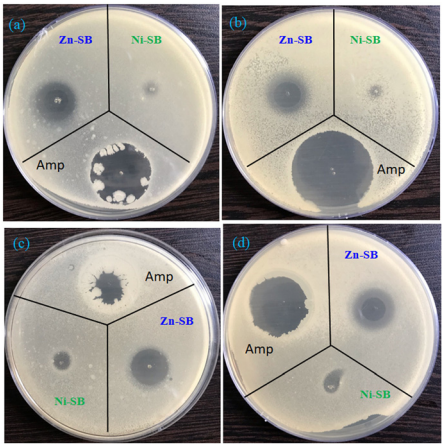

Fig. 6 Antibacterial prospect of the **Ni–SB** and **Zn–SB** metallogels against the Gram-negative bacteria (a) *Klebsiella pneumoniae* (MTCC 109), (b) *Vibrio parahaemolyticus*, and Gram-positive bacteria (c) *Staphylococcus aureus* (MTCC 96), (d) *Bacillus cereus* (MTCC 1272).

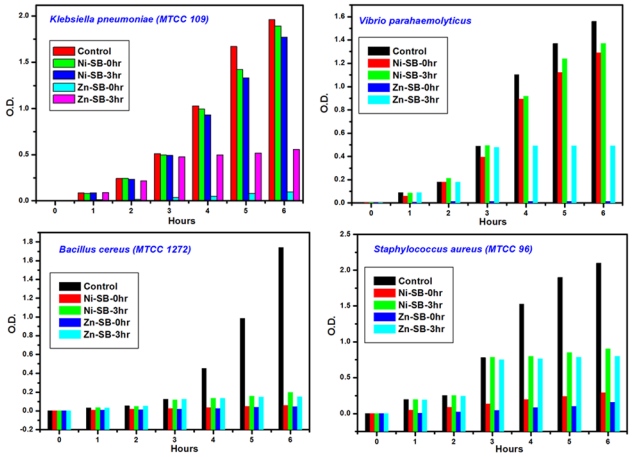

Fig. 7 Bacterial growth plots of Gram-positive and Gram-negative bacteria in TGE medium in the presence of **Ni–SB** and **Zn–SB**.

and *S. aureus*. In the case of Gram-negative bacteria *Klebsiella pneumoniae* (MTCC 109) and *Vibrio parahaemolyticus*, only **Zn–SB** elicited its antibacterial proficiency (Fig. 6). The **Zn–SB** metallogel exhibited higher antibacterial proficiency than **Ni–SB**. The minimum inhibitory concentration (MIC) for **Zn–SB** was ~75 μg mL^{-1} for both Gram-positive and Gram-negative bacteria, while the MIC for **Ni–SB** was found to be ~300 μg mL^{-1} for Gram-positive bacteria, which is approximately 4-fold higher than that of **Zn–SB**.

The differences in the antibacterial activity of **Ni–SB** against Gram-positive and Gram-negative bacteria are probably due to the differences in their cell wall structure. The outer layer (lipopolysaccharide layer) of the Gram-negative bacterial cell wall consists mainly of lipids. Therefore, the cell wall surface is inherently hydrophobic, which in turn retards the access of the inhibitory molecules. This leads to the loss of activity against the Gram-negative bacteria in contrast to Gram-positive bacteria, which has the outer layer of the cell wall consisting of peptide glycan.

During analysis, the mode of action (lethal/inhibitory) of both metallogels (*i.e.*, **Ni–SB** and **Zn–SB**) was found to be growth-inhibitory. Treatment of the growing cultures with the gel suspension at MIC results in growth inhibition, and this has been evidenced from spectrophotometric analysis (Fig. 7). Moreover, these were found to be viable, as evidenced by the obtained CFUs of the treated cells on a TGE-agar plate. This further ratifies that the metallogels (*i.e.*, **Ni–SB** and **Zn–SB**) are not lethal to the cells, but inhibit the growth of the bacteria.

3.5. Fabrication of the Schottky device and electrical measurements

A Schottky device obtained from these synthesized metallogels was fabricated through sandwich configuration, along with the ITO/metallogel/Al structure. Prior to device fabrication, indium tin oxide (ITO)-coated glass substrates were thoroughly washed employing soap solution, acetone, ethanol, and distilled water sequentially in an ultrasonic bath, and then properly dried. To establish the metal-semiconductor junction, aluminum was selected as the rectifier metal contact.

At an applied bias voltage and within the limit of ±1 V current, the current density–voltage (*J–V*) characteristic was calculated deliberately employing a Keithley 2635B source meter *via* two-probe technique for electrical characterization of the device. The Schottky diode's conductivity measurements were performed under dark conditions. All of these analyses were performed at room temperature.

Fig. 8 depicts the current density (*J*) *vs.* voltage (*V*) plots that were precisely measured in dark and light environments. The nature of the *J–V* characteristic is similar for both gel samples, *i.e.*, **Ni–SB** and **Zn–SB**. They exhibit a considerable amount of non-linearity in the scan voltage range, except for the current density, implying a non-ohmic conduction mechanism. This exhibited characteristic feature is similar to that of the Schottky

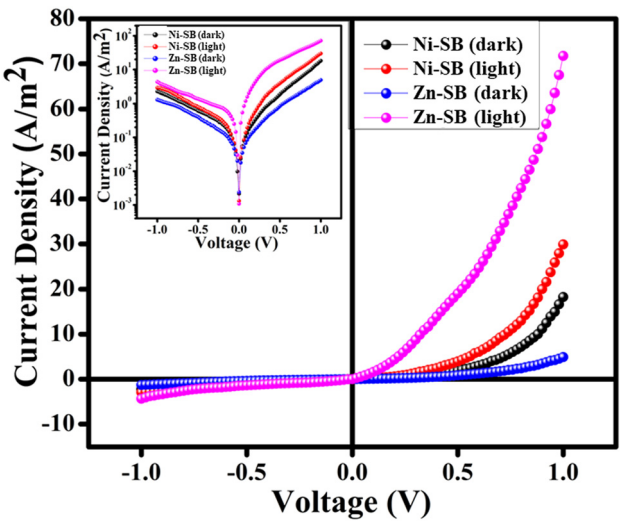

Fig. 8 Current Density–Voltage (*J–V*) graph of **Ni–SB** and **Zn–SB** under dark & light conditions. The insets show the respective *J vs. V* plots (in log scale).

Table 1 Electrical parameters of the **Ni–SB** and **Zn–SB**-based Schottky barrier diodes

Sample	On/off Ratio	Rectifi-cation Ratio	Condu-ctivity (s m^{-1})	Series resistance (Ω) from $dV/d\ln J$ *vs.* J curve	Series resistance (Ω) from H *vs.* J curve	Ideality factor (η)	Barrier height φ_b (eV)
Ni–SB (dark)	1.64	8.04	2.62×10^{-6}	18.90 K	18.83 K	3.00	0.74
Ni–SB (Light)		10.20	5.55×10^{-6}	9.00 K	8.84 K	2.40	0.73
Zn–SB (Dark)	14.63	3.74	1.18×10^{-6}	36.15 K	37.34 K	3.93	0.75
Zn–SB (Light)		16.45	3.32×10^{-5}	2.05 K	2.03 K	2.14	0.69

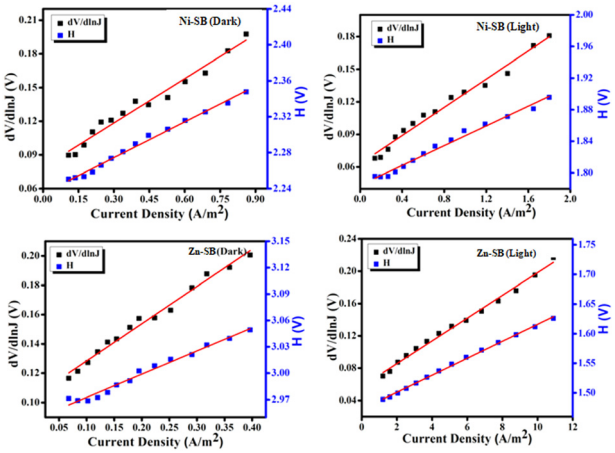

Fig. 9 Under dark and light conditions, $dV/d\ln J$ *vs.* J and H (J) *vs.* J curves in double y-axis for **Ni–SB** and **Zn–SB**.

barrier diode's rectification. In dark conditions, the device fabricated by means of **Ni–SB** exhibits a larger current density. However, in the presence of light, the device based on **Zn–SB** shows a higher on/off ratio (Fig. 8).

The rectification ratios were carefully analyzed for dark and light conditions. The calculated values are obtained as 8.04 (dark condition) and 10.20 (light condition) for the **Ni–SB**-based diode device. Whereas for the **Zn–SB**-based diode device, the values are found to be 3.74 (dark) and 16.45 (light). On the basis of the estimated conductivities, the devices fabricated based on **Ni–SB** and **Zn–SB** at room temperature reveal that the **Ni–SB**-based device has better conductivity (Table 1) under dark condition, whereas the **Zn–SB**-based device exhibits better conductivity in the presence of light. This is one of the essential and vital characteristics of the materials that are utilized in photovoltaic applications.

Based on Thermionic Emission (TE) Theory and Cheung's Method, the J–V characteristics of the Schottky diode were further studied carefully to extract the diode parameters[88,89] (Please see ESI† for details).

The plots of $dV/d\ln(J)$ *vs.* J in Fig. 9 are found to be linear. The y-axis intercept of this figure yields the ideality factors (η) of the SBDs. The diodes' barrier height (φ_b) is calculated from the y-axis intercept of the H (J) *vs.* J linear plots shown in Fig. 9. Table 1 shows the measured ideality factor and barrier height for the Al/metallogels junction in both dark and light conditions. The ideality factors for both metallogels-based devices deviated from unity, as observed.

Multiple generation recombinations of charge carriers in the junction region *via* interface traps and inhomogeneous barrier height is the cause of the variation.[90] However, it should be observed that the ideality factor of the devices under light condition is nearing unity. This indicates that there is less interfacial charge recombination at the junction, and that Schottky junctions have superior barrier uniformity.[91] The calculated barrier heights for the Al/metallogels junctions are 0.74 eV and 0.73 eV for **Ni–SB**, and 0.75 eV and 0.69 eV for **Zn–SB**, under dark and light conditions, respectively. As a result of these experimental outcomes, **Zn–SB** under light condition emerged as a better contender in terms of electrical conductivity than **Ni–SB**.

4. Conclusions

Fabrication of soft-scaffolds with sebacic acid and integration of metal ions Ni(II) and Zn(II) offer a smart strategy to functionalize the resulting metallogels. Supramolecular interactions are critically responsible for the outcome of such diverse morphological patterns, as obtained in these metallogel scaffolds. Both metallogels exhibit their intrinsic viscoelasticities, as evident from several rheological parameters. The thixotropic nature of these two metallogels offers an additional benefit. Utilization of a low molecular weight organic gelator like sebacic acid offers an economically cost-effective avenue. Supramolecular interactions operating within metallogel systems are critically responsible for the reflection of such diverse macroscopic properties. FESEM microstructural analysis exhibited the presence of different morphological patterns in these soft scaffolds. EDX elemental analyses were performed for both metallogels to confirm the presence of all elements derived from their constituents. IR spectroscopic analysis highlighted the possible noncovalent interactions in both metallogel systems. Antibacterial prospects of both metallogels were tested against Gram-negative and Gram-positive bacteria. For both cases, **Zn–SB** exhibited better results than the **Ni–SB** metallogel. The **Ni–SB** metallogel was found to be selective in terms of its antibacterial aspect. MIC for **Ni–SB** was found to be $\sim$300 μg mL^{-1} for Gram-positive bacteria, which is approximately 4-fold higher than that of **Zn–SB**. The growth inhibitory action of **Ni–SB** and **Zn–SB** towards the mentioned pathogens was visualized by spectrophotometric analysis. Apart from biorelevant importance, both metallogels were utilized for junction-type Schottky diode device-fabrication through sandwich configuration, along with the ITO/metallogel/Al structure.

Both devices exhibit non-ohmic type electrical conduction. The nature of the *J–V* characteristics is similar for both cases, exhibiting a considerable amount of non-linearity in the scanned voltage-range except for current density, implying a non-ohmic conduction mechanism. This characteristic feature is similar to that of the Schottky barrier diode's rectification. The device fabricated by means of the **Ni–SB**-based system exhibits a larger current density than **Zn–SB** under dark environment, whereas the device based on **Zn–SB** shows a higher on/off ratio with respect to **Ni–SB** in the presence of light. Based on these two potential functionalities obtained from the low molecular weight gelator of sebacic acid-directed supramolecular metallogel systems, it can be proposed that our synthesized metallogel materials may unveil a new possibility towards the domain of bio-electronics.

Conflicts of interest

The authors declare no competing financial interest.

Acknowledgements

B. D. thankfully acknowledges WBDSTBT (Govt. of West Bengal, India) for a research project (Sanction letter No.: 14(Sanc.)/ST/P/S&T/15G-18/2018 dated 29/01/2019) for financial support. G. L. is thankful to UGC, New Delhi for awarding him UGC-JRF (Award letter No-16-9 (June 2019)/2019 (NET/CSIR) UGC-Ref.: 208/(CSIR-UCG NET June 2019). S. M. is grateful to CSIR, New Delhi for awarding him CSIR-SRF (File No-09/202(0079)/2018-EMR-I.). B. Pal gratefully acknowledges the financial support of this work by DST-INSPIRE, GOI.

Notes and references

1 J.-M. Lehn, *Chem. Soc. Rev.*, 2017, **46**, 2378.
2 L. Arnedo-Sánchez, S. Bhowmik, S. Hietala, R. Puttreddy, M. Lahtinen, L. D. Colad and K. Rissanen, *Dalton Trans.*, 2017, **46**, 7309.
3 Q. Li, W. Zhang, O. Š. Miljanić, C.-H. Sue, Y.-L. Zhao, L. Liu, C. B. Knobler, J. F. Stoddart and O. M. Yaghi, *Science*, 2009, **325**, 855–859.
4 D. Fujita, K. Suzuki, S. Sato, M. Yagi-Utsumi, Y. Yamaguchi, N. Mizuno, T. Kumasaka, M. Takata, M. Noda, S. Uchiyama, K. Kato and M. Fujita, *Nat. Commun.*, 2012, **3**, 1093.
5 Y. Inokuma, S. Yoshioka and M. Fujita, *Angew. Chem., Int. Ed.*, 2010, **49**, 8912–8914.
6 M. Burnworth, L. Tang, J. R. Kumpfer, A. J. Duncan, F. L. Beyer, G. L. Fiore, S. J. Rowan and C. Weder, *Nature*, 2011, **472**, 334–337.
7 M. Martínez-Calvo, O. Kotova, M. E. Möbius, A. P. Bell, T. McCabe, J. J. Boland and T. Gunnlaugsson, *J. Am. Chem. Soc.*, 2015, **137**, 1983–1992.
8 H. Bunzen, E. Kalenius, S. Hietala and E. Kolehmainen, *Chem. – Eur. J.*, 2013, **19**, 12978–12981.
9 Z. Fang, P. Li and G. Yu, *Adv. Mater.*, 2020, **32**, 2003191.
10 H. B. Aiyappa, S. Saha, P. Wadge, R. Banerjee and S. Kurungot, *Chem. Sci.*, 2015, **6**, 603–607.
11 S. Majumdar, B. Pal, R. Sahu, K. S. Das, P. P. Ray and B. Dey, *Dalton Trans.*, 2022, **51**, 9007–9016.
12 S. Dhibar, A. Dey, S. Majumdar, A. Dey, P. P. Ray and B. Dey, *Ind. Eng. Chem. Res.*, 2020, **59**, 5466–5473.
13 S. Majumdar, P. P. Ray, R. Sahu, A. Dey and B. Dey, *Int. J. Biol. Macromol.*, 2022, **195**, 287–293.
14 S. Dhibar, A. Dey, S. Majumdar, D. Ghosh, A. Mandal, P. P. Ray and B. Dey, *Dalton Trans.*, 2018, **47**, 17412–17420.
15 S. Majumdar, T. Singha, S. Dhibar, A. Mandal, P. K. Datta and B. Dey, *ACS Appl. Electron. Mater.*, 2020, **2**, 3678–3685.
16 G. Lepcha, T. Singha, S. Majumdar, A. K. Pradhan, K. S. Das, P. K. Datta and B. Dey, *Dalton Trans.*, 2022, **51**, 13435.
17 A. Adhikary, K. S. Das, S. Saha, M. Roy and R. Mondal, *Dalton Trans.*, 2020, **49**, 13487–13495.
18 N. Zhang, J. Lock, A. Sallee and H. Liu, *ACS Appl. Mater. Interfaces*, 2015, **7**, 20987–20998.
19 A. Ghadban, A. S. Ahmed, Y. Ping, R. Ramos, N. Arfin, B. Cantaert, R. V. Ramanujan and A. Miserez, *Chem. Commun.*, 2016, **52**, 697–700.
20 W. Zhao, K. Odelius, U. Edlund, C. Zhao and A.-C. Albertsson, *Biomacromolecules*, 2015, **16**, 2522–2528.
21 L. Yan, S. Gou, Z. Ye, S. Zhanga and L. Ma, *Chem. Commun.*, 2014, **50**, 12847.
22 P. Terech, M. Yan, M. Marechal, G. Royal, J. Galvez and S. K. P. Velu, *Phys. Chem. Chem. Phys.*, 2013, **15**, 7338.
23 M. Häring and D. DíazDíaz, *Chem. Commun.*, 2016, **52**, 13068.
24 B. Xing, M.-F. Choi and B. Xu, *Chem. – Eur. J.*, 2002, **8**, 5028–5032.
25 T. Zhao, S. Chen, K. Kang, J. Ren and X. Yu, *Langmuir*, 2022, **38**, 1398–1405.
26 W. Fang, Y. Zhang, J. Wu, C. Liu, H. Zhu and T. Tu, *Chem. – Asian J.*, 2018, **13**, 712–729.
27 S. Sarkar, P. K. Maji, Y. Negishi, S. Dutta, T. N. Das, R. Pan and S. Sarkar, *ACS Appl. Nano Mater.*, 2021, **4**, 1455–1466.
28 K. Sarkar, H. K. Datta, S. Ahmed and P. Dastidar, *ChemistrySelect*, 2021, **6**, 13992–14004.
29 P. M. Shukla, G. Kaul, S. Chopra and S. Verma, *ChemistrySelect*, 2019, **4**, 1834–1839.
30 P. Biswas, H. K. Datta and P. Dastidar, *Chem. Commun.*, 2022, **58**, 969–972.
31 H. T. P. Anh, C.-M. Huang and C.-J. Huang, *Sci. Rep.*, 2019, **9**, 11562.
32 S. Majumdar, G. Lepcha, K. T. Ahmed, I. Pal, S. R. Biswas and B. Dey, *J. Mol. Liq.*, 2022, **368**, 120619.
33 A. Sebastian and E. Prasad, *Langmuir*, 2020, **36**, 10537–10547.
34 Q. Lin, T.-T. Lu, X. Zhu, B. Sun, Q.-P. Yang, T.-B. Wei and Y.-M. Zhang, *Chem. Commun.*, 2015, **51**, 1635–1638.
35 S. Sarkar, S. Dutta, S. Chakrabarti, P. Bairi and T. Pal, *ACS Appl. Mater. Interfaces*, 2014, **6**, 6308–6316.
36 H. Yao, Y.-B. Niu, Y.-P. Hu, X.-W. Sun, Q.-P. Zhang, Y.-M. Zhang, T.-B. Wei and Q. Lin, *New J. Chem.*, 2022, **46**, 17251–17259.

37 Y. Yang, W. Liu, Q. Zhong, J. Zhang, B. Yao, X. Lian and H. Niu, *ACS Appl. Nano Mater.*, 2021, **4**, 4735–4745.
38 Q. Feng, K. Wan, T. Zhu, X. Fan, C. Zhang and T. Liu, *ACS Appl. Mater. Interfaces*, 2022, **14**, 4542–4551.
39 Q. Lin, B. Sun, Q.-P. Yang, Y.-P. Fu, X. Zhu, T.-B. Wei and Y.-M. Zhang, *Chem. – Eur. J.*, 2014, **20**, 11457–11462.
40 S. Mondal, N. Alam, S. Sahoo and D. Sarma, *J. Colloid Interface Sci.*, 2023, **633**, 441–452.
41 S. Sarkar, S. Dutta, P. Bairi and T. Pal, *Langmuir*, 2014, **30**, 7833–7841.
42 K. Mitsumoto, J. M. Cameron, R.-J. Wei, H. Nishikawa, T. Shiga, M. Nihei and H. A. Oshio, *Chem. – Eur. J.*, 2017, **23**, 1502–1506.
43 F. Fages, *Angew. Chem., Int. Ed.*, 2006, **45**, 1680.
44 M.-O. M. Piepenbrock, N. Clarke and J. W. Steed, *Langmuir*, 2009, **25**, 8451–8456.
45 S. C. Zacharias, G. Ramon and S. A. Bourne, *Soft Matter*, 2018, **14**, 4505–4519.
46 Z. Sun, F. Lv, L. Cao, L. Liu, Y. Zhang and Z. Lu, *Angew. Chem., Int. Ed.*, 2015, **54**, 7944–7948.
47 X. Wang, T. He, L. Yang, H. Wu, R. Zhang, Z. Zhang, R. Shen, J. Xiang, Y. Zhang and C. Wei, *Nanoscale*, 2016, **8**, 6479–6483.
48 B. Yao, H. Wang, Q. Zhou, M. Wu, M. Zhang, C. Li and G. Shi, *Adv. Mater.*, 2017, **29**, 1700974.
49 H. Svobodová, M. Lahtinen, Z. Wimmer and E. Kolehmainen, *Soft Matter*, 2012, **8**, 7840–7847.
50 J. Yang, F. Xu and C.-R. Han, *Biomacromolecules*, 2017, **18**, 1019–1028.
51 E. Degtyar, M. J. Harrington, Y. Politi and P. Fratzl, *Angew. Chem., Int. Ed.*, 2014, **53**, 12026.
52 J. Nanda, B. Adhikari, S. Basak and A. Banerjee, *J. Phys. Chem. B*, 2012, **116**, 12235–12244.
53 W. Weng, J. B. Beck, A. M. Jamieson and S. J. Rowan, *J. Am. Chem. Soc.*, 2006, **128**, 11663–11672.
54 A. Y. Tam and V. W. Yam, *Chem. Soc. Rev.*, 2013, **42**, 1540–1567.
55 N. Lanigan and X. Wang, *Chem. Commun.*, 2013, **49**, 8133–8144.
56 R. Tatikonda, K. Bertula, S. Hietala, K. Rissanen and M. Haukka, *Dalton Trans.*, 2017, **46**, 2793–2802.
57 P. Dastidar, *Chem. Soc. Rev.*, 2008, **37**, 2699–2715.
58 I. Torres-Moya, A. Sánchez, B. Saikia, D. S. Yufit, P. Prieto, J. R. Carrillo and J. W. Steed, *Gels*, 2023, **9**, 26.
59 M. Suzuki and K. Hanabusa, *Chem. Soc. Rev.*, 2009, **38**, 967–975.
60 S. Majumdar, A. Dey, R. Sahu, G. Lepcha, A. Dey, P. P. Ray and B. Dey, *Mater. Res. Bull.*, 2023, **157**, 112003.
61 S. Majumdar, G. Lepcha, R. Sahu and B. Dey, *J. Phys. Chem. Solids*, 2022, **170**, 110903.
62 A. Dey, S. Sil, S. Majumdar, R. Sahu, M. Ghosh, G. Lepcha, P. P. Ray and B. Dey, *J. Phys. Chem. Solids*, 2022, **160**, 110300.
63 S. Majumdar, S. Sil, R. Sahu, M. Ghosh, G. Lepcha, A. Dey, S. Mandal, P. P. Ray and B. Dey, *J. Mol. Liq.*, 2021, **338**, 116769.
64 S. Dhibar, A. Dey, S. Majumdar, P. P. Ray and B. Dey, *Int. J. Energy Res.*, 2021, **45**, 5486–5499.
65 S. Dhibar, A. Dey, D. Ghosh, S. Majumdar, A. Dey, P. Mukherjee, A. Mandal, P. P. Ray and B. Dey, *ChemistrySelect*, 2019, **4**, 1535–1541.
66 P. Das, S. Majumdar, A. Dey, S. Mandal, A. Mondal, S. Chakrabarty, P. P. Ray and B. Dey, *New J. Chem.*, 2021, **45**, 15920–15927.
67 S. Dhibar, R. Jana, P. P. Ray and B. Dey, *J. Mol. Liq.*, 2019, **289**, 111126.
68 Y. Zhang, F. Shen, Y. Li, X.-L. Pang, C. Zhang, J. Ren and X. Yu, *Chem. Commun.*, 2020, **56**, 2439–2442.
69 L. Ye, L. Wan and F. Huang, *New J. Chem.*, 2017, **41**, 4424–4430.
70 J. H. Lee, S. Kang, J. Y. Lee and J. H. Jung, *Soft Matter*, 2012, **8**, 6557–6563.
71 R. Kyarikwal, N. Malviya, A. Chakraborty and S. Mukhopadhyay, *ACS Appl. Mater. Interfaces*, 2021, **13**, 59567–59579.
72 C. Rizzo, S. Marullo, F. Billeci and F. D'Anna, *Eur. J. Org. Chem.*, 2021, 3148–3169.
73 H. Wu, J. Zheng, A.-L. Kjøniksen, W. Wang, Y. Zhang and J. Ma, *Adv. Mater.*, 2019, **31**, 1806204.
74 P. Biswas and P. Dastidar, *Inorg. Chem.*, 2021, **60**, 3218–3231.
75 K. Sarkar, H. K. Datta, S. Ahmed and P. Dastidar, *ChemistrySelect*, 2021, **48**, 13992–14004.
76 K. Sarkar and P. Dastidar, *Chem. – Asian J.*, 2019, **14**, 194–204.
77 M. Tao, K. Xu, S. He, H. Li, L. Zhang, X. Luo and W. Zhong, *Chem. Commun.*, 2018, **54**, 4673–4676.
78 I. Djordjevic, N. R. Choudhury, N. K. Dutta and S. Kumar, *Polym. Int.*, 2011, **60**, 333–343.
79 J. Kim, K.-W. Lee, T. E. Hefferan, B. L. Currier, M. J. Yaszemski and L. Lu, *Biomacromolecules*, 2008, **9**, 149–157.
80 Y. In, U. Amornkitbamrung, M.-H. Hong and H. Shin, *ACS Omega*, 2020, **5**, 27204–27210.
81 W. Lin, Z. Ling, Z. Zhang and X. Fang, *J. Energy Storage*, 2020, **32**, 101849.
82 X. Liu, L. Lebrun, N. Follain and N. Desilles, *Mater. Adv.*, 2022, **3**, 389–398.
83 R. Paul, M. Singh, V. VJ, G. Manik and S. K. Sahoo, *Ind. Eng. Chem. Res.*, 2023, **62**, 423–434.
84 S. R. Biswas, P. Ray, M. C. Johnson and B. Ray, *Appl. Environ. Microbiol.*, 1991, **57**, 1265–1267.
85 T. A. Kazi, S. Mitra, B. C. Mukhopadhyay, S. Mandal and S. R. Biswas, *Gene*, 2021, **777**, 145459.
86 T. A. Kazi, B. C. Mukhopadhyay, S. Mandal and S. R. Biswas, *Gene*, 2023, **856**, 147154.
87 B. C. Mukhopadhyay, S. Mitra, T. A. Kazi, S. Mandal and S. R. Biswas, *Microbiol. Resour. Announce.*, 2019, **8**, e01480.
88 S. Halder, B. Pal, A. Dey, S. Sil, P. Das, A. Biswas and P. P. Ray, *Mater. Res. Bull.*, 2019, **118**, 110507.
89 S. K. Cheung and N. W. Cheung, *Appl. Phys. Lett.*, 1986, **49**, 85–87.
90 R. Jana, J. Datta, S. Sil, A. Dey, B. Pal, A. Biswas and P. P. Ray, *Mater. Res. Express*, 2019, **6**, 1050d1.
91 P. Das, B. Pal, J. Datta, M. Das, S. Sil and P. P. Ray, *J. Phys. Chem. Solids*, 2021, **148**, 109706.